Quantum films adsorbed on graphite: Third and fourth helium layers

Marlon Pierce and Efstratios Manousakis
Department of Physics and Center for Materials Research and Technology, Florida State University, Tallahassee, Florida 32306-4350
(Received 18 August 2000; published 23 March 2001)

Using a path-integral Monte Carlo method for simulating superfluid quantum films, we investigate helium layers adsorbed on a substrate consisting of graphite plus two solid helium layers. The solid helium layers are modeled first as inert, with paths frozen at equilibrated positions, and then as active, with second-layer atoms included in the Monte Carlo updating. In both cases, we observe the formation of as many as three well defined additional layers above the first two and determine the layer promotion density by calculating the density profile and through a calculation of the chemical potential. For liquid layers adsorbed onto the inert solids, we find self-bound liquid phases in both the third and fourth layers and determine the equilibrium density. In the third layer at coverages below equilibrium, we find liquid droplets and a metastable uniform liquid phase and determine the spinodal point that separates these regions. The above phases and their coverage ranges are in good agreement with several experiments. The superfluid density as a function of coverage is also calculated and it is observed to change only weakly around the promotion density. For coverages above the beginning of fourth-layer promotion, we observe continued increase in the third-layer density. We note that the third-layer density increase is perhaps enough to cause solidification in this layer, which would explain heat-capacity peaks observed experimentally for fourth layer coverages and would provide a simple explanation for the plateaus seen in the superfluid coverage. For helium adsorbed on an active second layer, we observe that a self-bound liquid phase occurs in the third layer and we determine the equilibrium density and spinodal point, which remain in agreement with experiment. We find that promotion to both the third and fourth layers is signaled by a change in the density dependence of the chemical potential. We further observe the increase in the second-layer density with increasing total coverage. The coverage dependence of the superfluid density is calculated and a pronounced drop is seen at high third-layer coverages as has also been observed experimentally.

DOI: 10.1103/PhysRevB.63.144524 PACS number(s): 67.70.+n, 67.40.Kh

I. INTRODUCTION

Helium films adsorbed on graphite exhibit a number of phases and have proven to be a rich source for both experimental and theoretical studies of two-dimensional phenomena. The graphite substrate is ordered on atomic length scales and offers a potential well for helium that is relatively strong for physical adsorption but is short ranged perpendicular to the substrate. As a result, a number of distinct, atomically thin layers occur each with its own phase diagram. Near the graphite surface, the layers tend to solidify with both commensurate and incommensurate solids occurring in the first two layers. In both the layers, this solidification occurs before promotion to the next layer. The second layer exhibits a coverage region with superfluidity as well[1–4] while the first layer apparently favors the formation of solid clusters over liquid droplets at low densities,[5–7] although there is a debate on this issue.[8,9] A general review of physically adsorbed films such as helium on graphite can be found in the book of Bruch, Cole, and Zaremba.[10] In this paper, we will focus on the liquid third and fourth layers.

Detailed information on the film structure at low temperatures for the third and higher layers has come from a number of experiments including heat capacity,[11,8] torsional oscillator,[1,2,12] and third sound measurements.[13] Ranges in which the heat capacity depends linearly on the coverage suggest that gas-liquid coexistence regions exist in the third and fourth layers. The transition from liquid droplets to a uniform liquid phase in each layer is signaled by a peak in the isothermal compressibility.[13] Unlike the first and second layers, these higher layers do not solidify before layer promotion since torsional oscillator measurements detect superfluidity for all coverages beginning at the intermediate third-layer densities. This apparently rules out earlier suggestions that the third layer may solidify,[8,13] although it still may be possible for solidification to take place under compression of higher layers.

Perhaps the most unusual feature of the higher layers is the steplike behavior of superfluidity with increasing density.[1,2] The superfluid coverage in layered films will not grow continuously because of the layering transitions. Plateaus in the superfluid density immediately after layer promotion are expected and have been observed when the particles are in the droplet region. These plateaus occur because the droplets in the new layer lack the connectivity to exhibit superflow across the entire surface.[14] The interesting observation is that the plateaus actually begin *before* layer promotion for the third through sixth layers. At 500 mK, superfluidity even exhibits a decrease with increasing coverage near the promotion to the fourth layer. These effects have been discussed in the context of the Bose-Hubbard model.[15] The suggestion is that the plateaus are produced by the increased localization of particles in the dense liquid.

Theoretical tools applied in the study of quantum films on realistically treated substrates include the hypernetted chain Euler-Lagrange (HNC-EL) method,[16–19] density functional theory,[20–22] and quantum Monte Carlo.[23–26,9,3,4] The HNC-EL approach has been used extensively in studies of

the third and higher layers of helium films on graphite. This approach determines stable coverages of the helium layers. Because the theory requires a uniform film, calculations cannot be made for all coverages. Breakdowns in the theory are interpreted as occurring at coverages where the film is unstable to the formation of droplet patches or to layer promotion. The theory predicts that at least three liquid layers will form on top of the solid first and second layers and yields a maximum coverage value before promotion of 0.065 atom/Å^2 for each layer, in good agreement with, but somewhat below, the experimental value of 0.076.[8,13]

In this paper we present results for the third and fourth helium layers using the path-integral Monte Carlo (PIMC) method. Our simulation is able to take into account the effect of the second layer's corrugations and zero-point motion on the third layer. We are also able to allow for the possibility of promotion and demotion of particles between the second, third, and fourth layers and these effects are observed. Finally, our simulation method can be applied to the entire range of possible phases in a layer, from liquid droplets to full solidification. Thus we are able to probe both the low density and high density phases of a layer.

II. SIMULATION METHOD

Our simulation is performed using a path-integral Monte Carlo method that includes particle permutations and substrate effects. The general method for bulk simulation has been reviewed elsewhere[27] and our modifications for simulating layered systems are given in a previous publication.[4] Some of the present calculations have required minor changes to this method, so we will briefly outline the procedure now in order to explain the modifications.

A. Overview of procedure

The partition function Z for a system of N bosons at the inverse temperature β can be expanded as a path-integral by inserting M intermediate configurations,

$$Z=\frac{1}{N!}\sum_{P}\int\cdots\int d^3R_1\cdots d^3R_M d^3R\,\rho(\mathbf{R}_1,\mathbf{R}_2;\tau)\times\rho(\mathbf{R}_2,\mathbf{R}_3;\tau)\cdots\rho(\mathbf{R}_M,P\mathbf{R}_1;\tau), \quad (1)$$

where ρ is the density matrix, $\mathbf{R}_i$ is a configuration of N particles, and $\tau=\beta/M$. The sum over P is the sum of all possible permutations of particle labels. Both the configurations and the permutations are sampled by our PIMC method. The number of intermediate configurations used M is referred to as the number of inverse-temperature slices.

To implement this method, two important ingredients are needed. First, a starting approximation for the density matrix at τ is required. The simplest of these is the so-called semiclassical approximation. The drawback to this approach is that very high starting temperatures are needed to obtain an accurate approximation. Methods for improving the starting approximation can lower the starting temperature to $\tau^{-1}=40$ K.[27]

The second important feature of the method is multilevel sampling. The path-integral, Eq. (1), can be thought of as a system of N ring polymers each with M beads. Particle permutations correspond to splicing the ring polymers together. In multilevel sampling, we update particle positions over a section of the polymer chain. This allows us to implement permutations by spreading them over several inverse-temperature slices. The number of slices to be updated is 2^l, where l is the level of the move. The value of l must be chosen to balance the acceptance of particle moves and particle permutations. Increasing the value of l increases the rate of accepting permutations but decreases the acceptance of new particle positions while decreasing l has the opposite effect. Typically, we take $l=3$ since this gives the optimum balance between the acceptance of permutations and new particle positions.

B. Third and higher layers

In our calculations for the third and higher layers, we use a simulation cell that is designed to accommodate the first layer helium solid. Periodic boundary conditions are applied in the plane of the substrate. We approximate the effects of the solid first layer on the second and higher-layer atoms by placing frozen atoms at triangular lattice sites on the substrate. These frozen atoms are located 2.8 Å above the graphite surface, the height of the first layer as indicated by neutron scattering.[28] The second layer also solidifies before promotion to the third layer occurs. In a previous simulation,[4] we determined that the highest second layer coverage before layer promotion was 0.2117 atom/Å^2. This simulation was performed with 20 second-layer atoms above 30 frozen first-layer atoms in a cell of dimensions 15.075 Å$\times$15.67 Å. The majority of our simulation results for the third and higher layers were obtained using a simulation cell of this size. The use of frozen and active layers to simulate quantum films using the PIMC method was first discussed by Wagner and Ceperley.[25,26] We discuss our own implementation and highlight its particular features below.

In order to investigate the effects of an inert versus active second layer, we have performed two sets of calculations. In the first, we equilibrate the second layer at 0.2117 atom/Å^2. The positions of these atoms are then frozen and are no longer included in the sampling. Additional atoms are then placed above this inert substrate and have their positions and permutations sampled. We refer to these additional atoms as being ''active.'' The bisection level used in this simulation was $l=3$. All errors that we report for these calculations are statistical errors arising from the Monte Carlo simulation of the active atoms above a particular frozen second layer. There will be additional systematic errors that arise from our particular choice for the frozen second-layer configuration.

In the second set of calculations, both the second and third-layer particles are included in the sampling. There is a potential problem with doing Monte Carlo calculations on such a system. The third layer is liquid and permutations will occur at low temperatures. This favors using $l=3$ for this layer. The second layer, on the other hand, is solid and furthermore increases in coverage as the overall coverage is

increased. Using $l=3$ produces, a low acceptance rate for particle moves in the compressed second layer. Sampling efficiency can be improved by using $l=2$ for this layer. Thus a single value of l for the entire system is not optimum.

To give each layer the best value of l, we have partitioned atoms into ''second-layer'' and ''third-layer'' atoms. The second-layer atoms have their positions initially taken from an equilibrated second-layer solid. The third-layer atoms are started from an initial configuration of atoms placed at various heights above the second layer. Promotion and demotion between the layers are allowed but the layer label of the atoms does not change. The third-layer atoms are sampled with $l_{3rd}=3$ while second-layer atoms are sampled at $l_{2nd}=2$. Permutations are allowed between atoms with the same layer label but we do not allow atoms with different layer labels to permute. This limitation is not a problem for atoms demoted to the second layer after being initially placed on the third layer since exchanges are uncommon in the solid second layer. The promotion of a particle from the second layer to the third occasionally occurs after a particularly long simulation. At most, only one particle is promoted, so this will have little effect on the permutations in the third layer in all but the lowest coverages. This approach gives a higher acceptance rate for second-layer-particle moves while allowing permutations to occur reasonably often in the third layer. We have found that this partitioning of l lowers the energy by an amount ranging from 0.0 K to 0.1 K per atom relative to energy calculations with a single value $l=3$ for the entire system. The smallest energy shift occurred at the lowest coverage tested, 0.2286 atom/Å^2. At this coverage the two values were within error bars. The greatest energy shift occurred near the equilibrium coverage of the third layer liquid. This was the highest coverage we tested. We also compared the energy values at selected coverages to calculations performed with a single value $l=2$ for the entire system and found them to agree, but third layer superfluidity was suppressed, as expected.

III. RESULTS FOR THE THIRD AND FOURTH LAYERS

Before presenting our simulation results, we wish to clarify the convention that we use to report adsorbed helium coverages. Normally, the values we give for the density are for the total adsorbed helium (first two solid layers plus any additional coverages for the higher layers). Relative coverages within a layer are prefaced with a reference to that layer. For example, the coverage 0.2583 atom/Å^2 using our standard simulation cell corresponds to a third layer coverage of 0.0466 atom/Å^2 plus two solid layers with a combined coverage of 0.2117 atom/Å^2.

A. Results with the inert second layer

1. Layer promotion and demotion

In order to study multiple layers of helium film, it is first necessary to establish that our simulation does, in fact, produce distinct layers with increasing coverage. This is illustrated in Fig. 1, which shows the growth of the density profile perpendicular to the substrate for the third and higher layers with increasing density. The peaks associated with the third and fourth layers can be clearly observed as can the beginning of the fifth-layer peak at the highest simulated coverage. Also, as can be seen in the figure, the continued growth of the third-layer peak for all coverages indicates compression of this layer even after atoms are promoted to the higher layers.

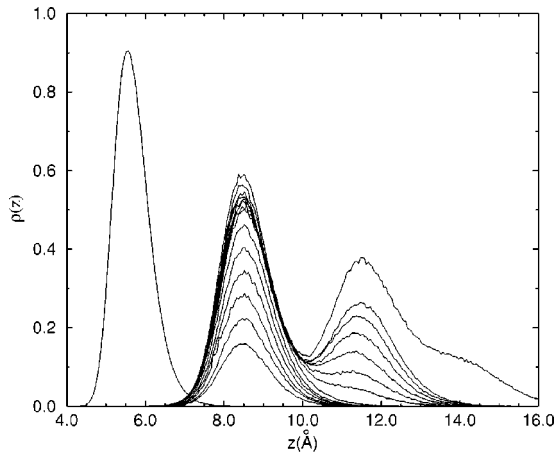

FIG. 1. Density profiles at 400 mK for the second, third, and fourth layers as a function of height above the graphite substrate. The leftmost peak is for the frozen, equilibrated second layer. The coverages shown begin at 0.2329 atom/Å^2 and increase in increments of 0.0085 up to 0.3345. The density profile for 0.3811 atom/Å^2 is also shown. The profiles are normalized so that integration gives the number of atoms.

Promotion to the fourth layer occurs for coverages greater than 0.2837 atom/Å^2 (17 active atoms). This coverage may be determined from the following observation, which is illustrated in Fig. 2. For coverages at and just below promotion, increasing the coverage increases the peak height but does not appreciably change the profile's width. Just above this density, the peak height does not change but an abrupt increase in the width is observed. With increasing coverage, the tail of the profile just above layer promotion evolves into

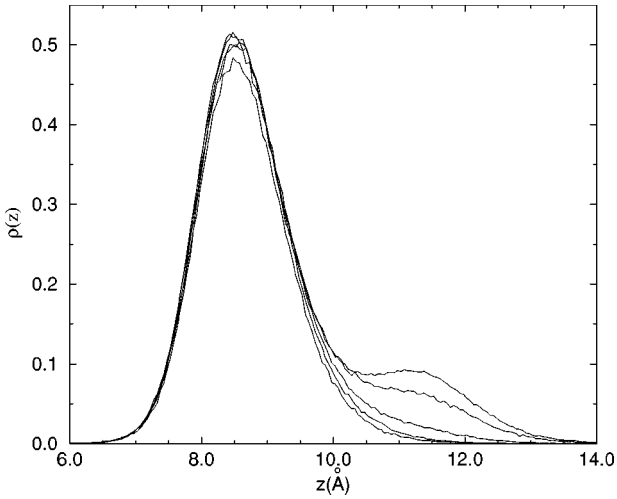

FIG. 2. Density profiles near layer promotion. The coverages are 0.2794, 0.2837, 0.2879, 0.2964, and 0.3005 atom/Å^2.

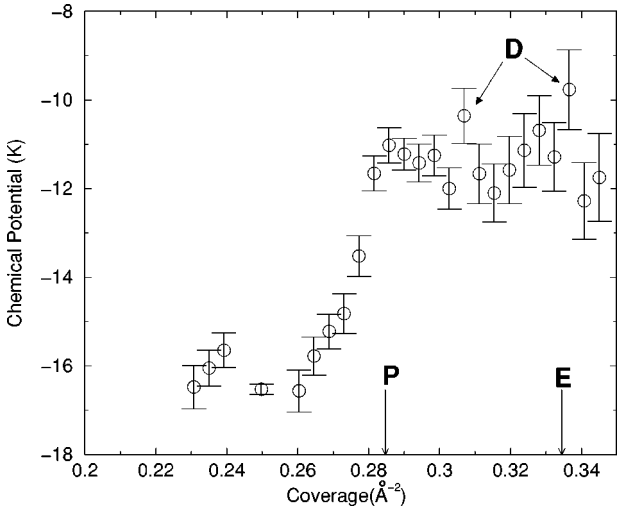

FIG. 3. Chemical potential for third and fourth layers. The arrows indicate the third layer promotion density (P) and the fourth layer equilibrium coverage (E). The densities denoted by D and the dark arrows are discussed in the text.

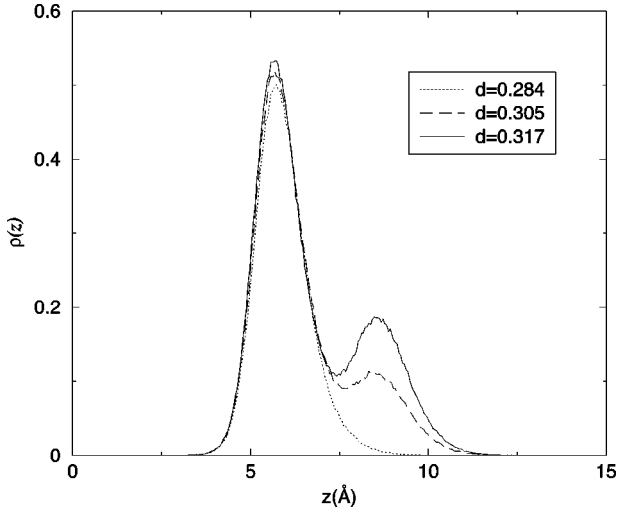

FIG. 4. Density profiles for the third and fourth layers. Coverages are given in Å^{-2}.

the fourth-layer peak. This is also illustrated in the figure. This value for layer promotion is in agreement with experiment. Heat capacity measurements[11,8] show layer promotion at 0.288 atom/Å^2 while isothermal compressibility measurements[13] give a somewhat lower value at 0.280 atom/Å^2 for the promotion density.

Layer promotion is also signaled by a change in the density dependence of the chemical potential. By differencing our calculated total energy values, we can obtain the chemical potential μ. This is plotted in Fig. 3. The values for the energy per particle are given in Table I. As can be seen from the figure, the chemical potential increases rapidly just below layer promotion until it becomes favorable to promote an atom to the next layer. Above layer promotion, the chemical potential remains roughly constant with increasing density, as it should for the liquid-gas-coexistence region. This change in the density dependence of μ together with the density profiles determine the promotion density.

The chemical potential for the third and fourth layers is shown in Fig. 3. As can be seen in the range 0.26–0.28 atom/Å^2 each additional atom causes a rapid increase in μ. Around 0.284 atom/Å^2, μ_3 of the third layer exceeds μ_4 of the fourth layer and so the next atom added to the system will be preferentially promoted to the fourth layer.

The beginning of particle promotion to a new layer does not signal the end of the filling of the old layer. As can be seen in Fig. 3, adding atoms to the system at the densities 0.306 and 0.334 atom/Å^2, marked by the letter D and the dark arrowheads, causes the chemical potential to increase above the chemical potential at layer promotion. Immediately above both these densities, μ drops back to values equal to μ at promotion. This signals particle demotion to the third layer. Figure 4 illustrates this for densities around 0.306. Notably, each additional demoted atom increases the

TABLE I. Energy/particle versus coverage at 400 mK for the third layer when the second layer is frozen. All the calculations use the 15.075 Å$\times$15.667 Å simulation cell. The number in parentheses gives the error in the last two three digits.

N	σ (Å^{-2})	E/N (K)	N	σ (Å^{-2})	E/N (K)
4	0.2286	−14.951(102)	20	0.2964	−14.774(18)
5	0.2329	−15.308(56)	21	0.3006	−14.602(13)
6	0.2371	−15.410(48)	22	0.3048	−14.479(17)
7	0.2413	−15.426(37)	23	0.3091	−14.307(22)
11	0.2583	−15.848(34)	24	0.3133	−14.193(18)
12	0.2625	−15.897(24)	25	0.3175	−14.105(19)
13	0.2667	−15.878(24)	26	0.3218	−14.015(23)
14	0.2710	−15.848(17)	27	0.3260	−13.905(21)
15	0.2752	−15.771(25)	28	0.3302	−13.787(19)
16	0.2794	−15.624(16)	29	0.3345	−13.707(20)
17	0.2837	−15.401(18)	30	0.3387	−13.573(23)
18	0.2879	−15.153(14)	31	0.3429	−13.528(17)
19	0.2921	−14.941(13)	32	0.3472	−13.478(27)

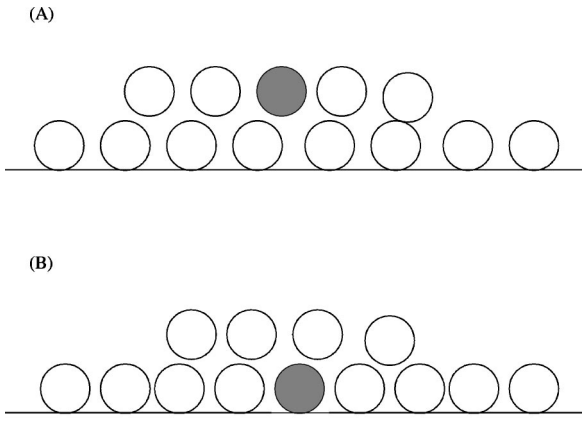

FIG. 5. An illustration of the circumstances of particle demotion. The shaded atom is added to the layered system. In (A), it joins the less dense outer layer. In (B), it is demoted to the more dense underlayer.

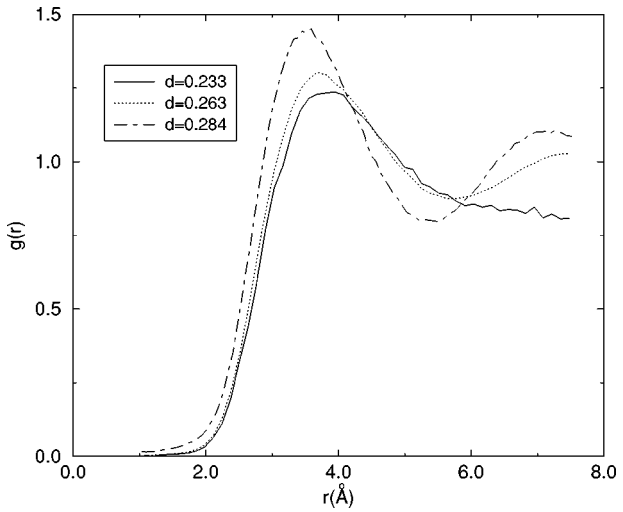

FIG. 6. The radial distribution function for the third layer at the indicated coverages, in atom/Å^2.

energy required to further increase the layer density, so μ at promotion is only a rough estimate of the chemical potential required to demote additional atoms.

Particle demotion may be understood as a balance between many factors. Atoms are initially promoted above a layer because this is energetically favorable. The first promoted atom loses the large energy benefit for being close to the substrate but gains kinetic energy since it is free to move about on the open surface with its wave function no longer constrained by the other atoms. It also retains some of the potential-energy advantage gained from having neighboring helium atoms. Adding more atoms to the system will favor the formation of droplets. However, once droplets have formed in the new layer, the next atom added to the system faces a different choice than the first promoted atom. This is illustrated in Fig. 5. If it goes into the less-dense outer layer, it gains some attraction from the other atoms in this layer. However, it no longer gains the kinetic-energy advantage that the first promoted atom had. On the other hand, if the added atom goes into the dense lower layer, it regains the benefit of being closer to the strongly attractive substrate. Furthermore, it has the energy advantage for having more helium neighbors: those in its layer, those in the layer above, and those in the layer below (not shown). In contrast, if the added atom goes into the outer layer, it has less neighbors. It should be noted that each demotion to the dense layer does significantly increase the chemical potential for this layer, so at some point it will be more favorable for atoms to be added to the outer layer again.

2. Third and fourth-layer phases

We expect four principal regions in the third layer before fourth-layer promotion. These are a low-density gas phase (which will have a negligible density at low temperatures), a droplet region, a metastable liquid region, and an equilibrium liquid phase. The droplet region consists of a liquid phase separated from a low-density gas by an interface. In the metastable region, the droplet phase is replaced by a stretched uniform phase that has a negative spreading pressure. The crossover from the droplet region to the stretched liquid phase occurs at the spinodal point. Direct evidence that the layer is liquid comes from torsional oscillator measurements, which detect superfluidity up to layer completion. The isothermal compressibility has been measured for the third and higher layers[13] and exhibits a divergence that is associated with the spinodal point. The equilibrium liquid coverage can be inferred from heat capacity measurements.[11] Below, we present evidence of each of these phases using several different observables.

First, we can establish the existence of droplets and a uniform liquid phase at different densities with the radial distribution function $g(r)$, which provides a direct probe of short and long-range behavior. Calculations for the third layer are shown in Fig. 6. These are plotted as functions of the magnitude of the distance vector between pairs of atoms projected onto the plane of the substrate. These calculations of the averaged $g(r)$ smooth out possible anisotropies induced by the corrugations of the underlying solid helium layer. The $g(r)$ for the three coverages shown in Fig. 6 are representative of the droplet region, the equilibrium liquid, and the liquid near layer promotion. At the lowest coverage, 0.233 atom/Å^2 (5 active atoms), the radial distribution function drops below unity at large distances as would be expected for a droplet phase. The actual dimensions of the droplet for a given density depend on the size of the simulation cell. For the intermediate coverage, 0.2624 atom/Å^2 (12 active atoms), the first peak has changed only slightly but the long-range behavior is noticeably different, rising again past unity instead of dropping continuously. At the highest coverage, 0.284 atom/Å^2, the system shows evidence of increased correlation but the long range-behavior cannot be determined due to the small size of the simulation cell. This largest coverage also has a different short-range behavior, showing an increased probability that the projected distance between two atoms will be less than 2.0 Å. In part, this is a result of the thickening of the layer as can be seen in Fig. 1. Because the atoms can be at different heights above the substrate, the projected distance between them can

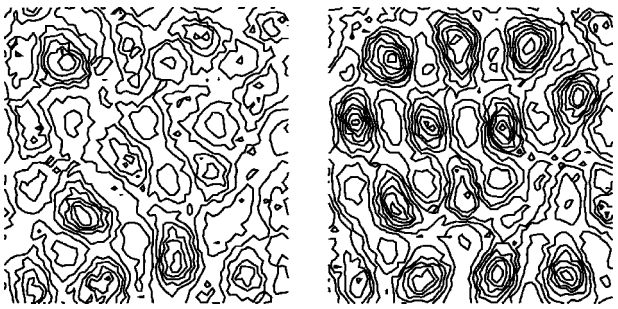

FIG. 7. Probability densities for the third-layer liquid near equilibrium (0.2625 atom/Å^2, left) and just before layer promotion (0.2837 atom/Å^2, right).

become smaller than would be possible in strictly two-dimensional calculations.

We can also gain some insight into the layer phases by examining contour plots of the probability distribution of atoms in the plane of the substrate. Plots near equilibrium and layer promotion are shown in Fig. 7. These plots show lines of equal probability for atomic positions averaged over several thousand Monte Carlo steps, so closely spaced lines show regions of relatively high probability while low-probability regions contain few contour lines. The high-density liquid shows noticeably more localization (separation into high- and low-density regions) than the equilibrium fluid. An increased correlation can also be seen in the radial distribution function at high density. This suggests that the system may be nearing a liquid-solid-coexistence phase. This is also seen from the structure factor, which is shown in Fig. 8 as a function of the magnitude of $k=\sqrt{k_x^2+k_y^2}$. Notice that there is a rather strong peak at $\vec{k}=(1{,}667,0.802)$ $(k=1.85)$ with a value of $S(k)=2.14$. The finite-size limitations of our calculation does not allow us to draw a firm conclusion about the presence of a solid or a coexistence between a liquid and a solid.

Having established that the third layer has gas-liquid and uniform liquid phases, we can next determine the equilibrium coverage ranges of these phases. This can be done by using the Maxwell construction. At low temperatures, the total energy and the total free energy are nearly equal, so coexistence regions may be identified by applying the Maxwell construction to the energy. The results for the low-temperature (400 mK) scans are shown in Fig. 9. We have verified that the energy values shown are effectively zero temperature results by recalculating some values at 500 mK. In all the cases, the calculations at the two temperatures agreed within error bars. The values shown in the figure have been shifted by the amount $N_{act}e_0$, where $e_0=-15.897\pm0.024$ is the minimum energy per particle and N_{act} is the number of active atoms in the simulation. At low temperatures, the gas phase will have zero coverage and thus zero total energy. We can thus draw a coexistence line between the beginning of the third layer, 0.2117 atom/Å^2, and the coverage with minimum energy per particle. This higher coverage is the equilibrium liquid density. We find this coverage to be 0.2625 atom/Å^2 $(N_{act}=12)$. The best chi-squared parabolic fit around this minimum gives 0.2645(9) atom/Å^2. The number in parenthesis is the error in the last digit. At this density the layer is completely covered by a uniform liquid. Below this value, the system enters the gas-liquid coexistence region. The energy values in the coexistence region lie above the coexistence line either because the liquid phase is unphysically uniform or because of the appreciable cost for creating a phase boundary in a finite-size system. The third layer equilibrium coverage, 0.0528(9) atom/Å^2, is comparable to (and slightly higher than) the equilibrium coverage found for the second layer, 0.0480(6) atom/Å^2.[3,4] For both the layers, simulated with the same-size cell, the energy minimum occurs when the system contains 12 atoms.

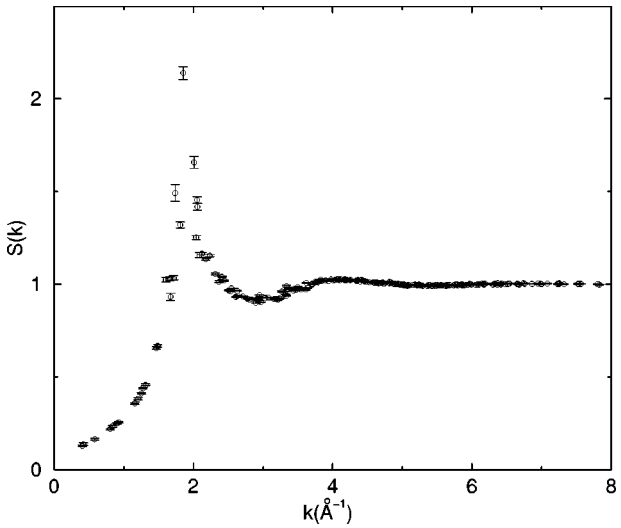

FIG. 8. The structure factor for the third layer just before layer promotion (0.2837 atom/Å^2).

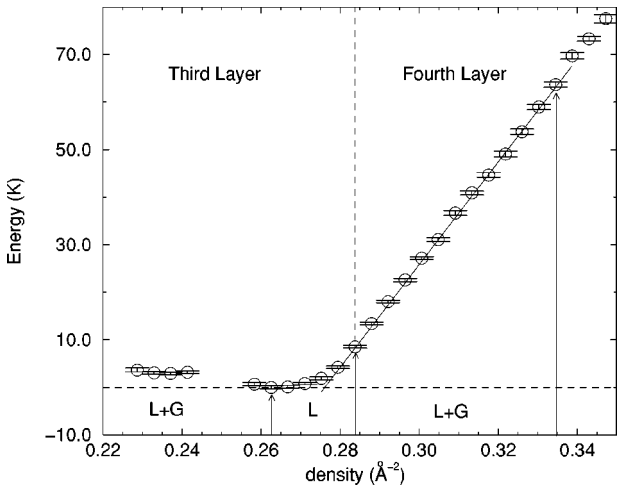

FIG. 9. Shifted total energy for the third and fourth layers. The horizontal dashed line is the gas-liquid-coexistence line for the third layer. The solid line is the gas-liquid-coexistence region for the fourth layer. The vertical dashed line gives the density of layer promotion. Gas-liquid (L+G) and uniform liquid (L) coverage ranges are indicated for both layers.

The equilibrium density that we determine is in good agreement with both heat capacity and torsional oscillator measurements. In the measurements of Greywall and

co-worker,[11,8] the low-temperature heat capacity depends linearly on density from the beginning of the third layer to 0.260 atom/Å^2. This linear dependence is a signal of phase coexistence.[29] The torsional oscillator measurements[2] provide evidence of a similar region. The temperature of the oscillator's dissipation peak, which gives a rough estimate for the superfluid transition temperature, is independent of coverage from 0.22 to 0.26 atom/Å^2. This is the characteristic of a surface covered by liquid droplets.[14] Increasing the coverage in the droplet region increases the size of the droplets, not their density and so the transition temperature remains constant.

For densities above the equilibrium coverage and below layer promotion, we have not been able to rule out the onset of solid-liquid coexistence in the third layer. Our procedure for identifying such regions in the second layer was to look for the instabilities in the total energy that signal phase coexistence. This was possible because that layer solidified before layer promotion. In the present case though, the energy cannot be used to find solid-liquid coexistence because any instabilities that might signal solidification are inextricably entangled with the liquid-vapor phase coexistence that occurs in the fourth layer at the same coverages. Specifically, layer promotion begins at the third layer coverage of 0.0720 atom/Å^2. The next increment in coverage that we can simulate using the cell described in Sec. II is 0.0762 atom/Å^2. In our previous simulation of the second layer using the same sized cell,[3,4] we determined that an incommensurate solid begins to form at the second layer coverage, 0.0762 atom/Å^2. Apparently, promotion preempts solidification. Also of note is that the density profile of the third layer at 0.0720 is much less peaked than the second layer at the same layer coverage, so any third-layer solid phase must have very large zero-point motion. One possible consequence of the third layer entering solid-liquid coexistence is that it may fully solidify under compression of further adsorbed layers. As we have discussed in the previous section, the third layer-density continues to increase even after fourth-layer promotion. Layer promotion is not a phase transition and can occur whenever the chemical potential of the system favors it. Thus it is possible to have layer promotion in the middle of a phase transition. The third layer solid-liquid-phase transition can be completed after fourth-layer promotion as additional atoms added to the system get demoted to the third layer. We note finally that there is some experimental evidence suggesting that third layer solidification may occur. In the heat-capacity results presented by Greywall,[8] a small peak at about 1.8 K can be observed for coverages beginning at 0.3100 atom/Å^2 between the rounded heat-capacity feature associated with the fourth-layer liquid and the sharp peak associated with the melting of the second-layer solid.

The fourth layer also exhibits a self-bound liquid coverage. We can identify this in the same manner as before. Since promotion to the fourth layer occurs above 0.2837 atom/Å^2, we can consider this coverage to correspond to a zero density fourth-layer gas. We apply the Maxwell construction again to the fourth layer and determine a bound liquid phase at 0.3345 atom/Å^2 (29 active atoms) giving a fourth-layer equilibrium density of 0.0508 atom/Å^2. The

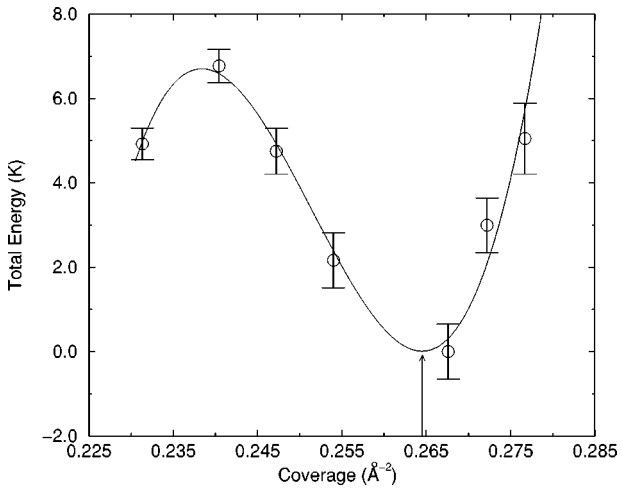

FIG. 10. Total energy for the third layer using the larger simulation cell described in the text. The solid curve is a fit to Eq. (2). The arrow indicates the equilibrium liquid coverage.

solid line in the figure gives the maximum possible range for gas-liquid coexistence in the fourth layer. All energy values in this region are on or above the coexistence line. This coexistence region agrees with heat capacity measurements,[8] which exhibit linear isotherms in the fourth layer up to 0.3300 atom/Å^2 at low temperatures.

A trend can be noticed in the equilibrium density as one progresses from the inner to the outer layers. For the first layer of helium adsorbed on a flat substrate, we have calculated the equilibrium density to be 0.0450(6) atom/Å^2, close to the two-dimensional value.[30] Successive increases are observed in the second and third layers as the zero-point motion of the layers perpendicular to the plane of the substrate becomes larger. From a two-dimensional point of view, this motion has the effect of softening the hard cores of the helium atoms.

In Fig. 9, we do not plot energy values for the coverages between 0.2413 and 0.2583 atom/Å^2 at 400 mK. Calculations that we performed for these densities at 500 mK actually showed an energy decrease, outside of error bars. We attribute this to variations inherent in using frozen configurations for the second layer: the two calculations required two different configurations and so there will be some systematic difference in the energy values.

We have repeated the third-layer calculations at 400 mK using a larger simulation cell (21.105 Å$\times$20.889 Å). This will allow us to examine finite-size effects and the effects of different configurations. We will also be able to examine the intermediate region that we excluded in the calculations using the smaller cell. The total energy values are given in Fig. 10. These energy values have been shifted by subtracting out the gas-liquid-coexistence line as described above. The energy per particle values used to construct this figure are given in Table II. The minimum energy per particle is -16.005 ± 0.027 K, which occurs at 0.2676 atom/Å^2 (24 atoms). We fit these energy values to a polynomial in the form

$$E/V = e_0 + B\left(\frac{\rho-\rho_0}{\rho_0}\right)^2 + C\left(\frac{\rho-\rho_0}{\rho_0}\right)^3, \qquad (2)$$

TABLE II. Energy/particle versus coverage at 400 mK above the frozen second layer using the 21.015 Å×20.889 Å simulation cell described in the text. The number in parentheses gives the error in the last two digits.

N	σ (Å^{-2})	E/N (K)
7	0.2291	−15.199(51)
8	0.2313	−15.362(47)
12	0.2404	−15.442(33)
15	0.2472	−15.689(36)
18	0.2540	−15.885(36)
24	0.2676	−16.005(27)
26	0.2722	−15.908(25)
28	0.2767	−15.833(30)

where ρ is the coverage. Fitted parameters are given in Table III. Not all digits are significant. Notable from the table is that the equilibrium liquid coverage occurs at the same density as in previous calculation with the smaller cell despite the fact that there is a small discrepancy in the energy values at similar coverages between the cells. In our previous calculations on the second layer, we observed that finite-size effects on the energy were negligible. Thus we believe that the difference in the minimum energy values obtained with the two cells is attributable to the particular frozen second-layer configurations that we used. We also observed that a calculation using the larger cell but at 500 mK and 0.2540 atom/Å^2 (18 active atoms) showed an energy increase over the value obtained at 400 mK.

By differencing the (unshifted) total energy values of the larger cell, we can obtain the chemical potential μ. Values obtained from both the fit and the actual energy values are shown in Fig. 11. The size of the chemical potential near the minimum (-16.88 K± 0.28) is, in general, in agreement with the value range of $-9--16$ K obtained for the third layer by Clements *et al.*[17] As noted by those authors, their values are sensitive to the attractiveness of their model substrate.

We can determine the spinodal point by taking the second derivative of Eq. (2). The isothermal compressibility is given by $\kappa_T=\rho^{-2}(\partial\mu/\partial\rho)_T^{-1}$, where ρ is the coverage. This diverges when the derivative of the chemical potential is zero. Below this coverage, $\partial\mu/\partial\rho$ is negative and the speed of sound becomes imaginary. This is the spinodal point. From the fit, we determine that this occurs at 0.2518 atom/Å^2, a third layer coverage of 0.0386 atom/Å^2. This is in agreement

TABLE III. Fitted parameters for the polynomial fit to the shifted total energy values.

Parameter	Value
e_0 (K)	0.0097±0.51
ρ_0 (Å^{-2})	0.2645±0.0005
B (K)	2057.3±237.0
C (K)	13885.7±1759.0
χ^2/ν	1.09

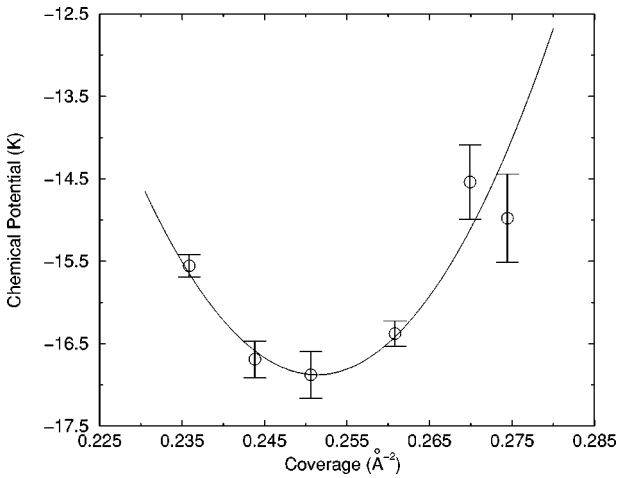

FIG. 11. Chemical potential calculated from the total energy values and the fit shown in Fig. 10.

with the HNC-EL calculations for the third layer.[17] Experimentally, the spinodal point can be determined from the divergence of the isothermal compressibility. In the third layer, this occurs near the third layer coverage of 0.03 atom/Å^2 at 1.2 K.[13]

The droplet region and the uniform coverage region for this simulation cell can be directly identified by the short-wavelength behavior of the static structure function $S(k)$. Figure 12 shows $S(k)$ for the coverages 0.2472 (below the spinodal point) and 0.2676 atom/Å^2 (near equilibrium). The upward swing of $S(k)$ for the lower density for small values of k indicates the presence of a droplet. Near the equilibrium density, the droplet has entirely covered the substrate and so $S(k\rightarrow 0)\rightarrow 0$.

B. Results with active second layer

1. Layer promotion and demotion

In the previous calculations we assumed that the solid second layer could be treated as inert, that is, the response of

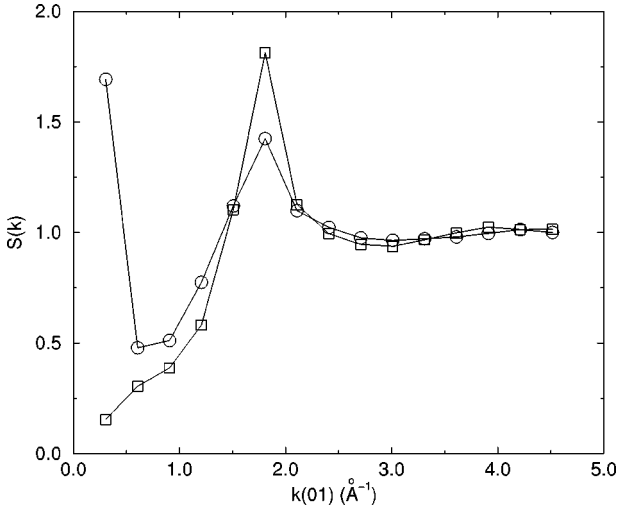

FIG. 12. Static structure factor at 0.2472 (circles) and 0.2676 atom/Å^2 (squares) at $T=400$ mK.

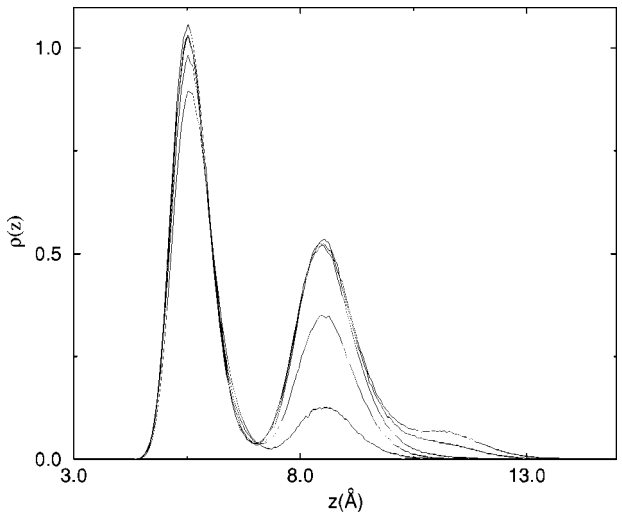

FIG. 13. Density profiles for the active second and third layers as a function of height above the substrate. The coverage values are 0.2296, 0.2625, 0.2879, 0.2964, and 0.3045 atom/Å^2.

the second-layer to the third was ignored. It is known experimentally, however, that the second-layer solid continues to be compressed after third-layer promotion. Evidence of this can be found in the heat-capacity peak associated with second layer melting.[8] This peak continues to increase in temperature for the entire range of the third layer indicating an increase in the second-layer density. Neutron scattering[28,31] also detects compression of the second layer by the third with an abrupt restructuring at intermediate third layer coverages. Second-layer compression is not unexpected since the compression of the first layer by the growth of the second is well established.[32] To allow for the effects of second-layer compression as well as the response of this layer to the growth of the third, we have performed calculations that include both the second and third-layer atoms in the Monte Carlo sampling.

Density profiles illustrate the compression of the second layer in our simulation. These are shown in Fig. 13 for selected coverages. The left and right peaks in the figure are for the second and third layers, respectively. As can be seen, the height of the second-layer peak grows between the coverage 0.2296 and 0.2879 atom/Å^2. The peak height then remains constant up to and including the coverage 0.2964 where promotion to the fourth layer is visible. Finally, the second-layer peak increases again at the highest coverage examined, 0.3049 atom/Å^2.

By integrating the profiles up to the minimum between the two peaks (at approximately 7.5 Å), we obtain the second layer coverages of 0.0845, 0.0885, 0.0894, 0.0890, and 0.0929 atom/Å^2 for the coverages shown in the figure. Thus at the lowest third-layer densities, no demotion occurs. Beginning at the intermediate coverages and up to layer promotion, a single atom is demoted. At low fourth layer coverages (the highest coverage examined) two atoms are demoted. As a consequence of demotion, promotion to the fourth layer is pushed to a higher overall coverage. As is illustrated in Fig. 13, we do not observe promotion to the fourth layer until the density has exceeded 0.2879 atom/Å^2 compared to 0.2837 atom/Å^2 when the second layer was frozen. This value will be further established below by examining the density dependence of the chemical potential. This value is still in agreement with the heat capacity[8] and isothermal compressibility[13,2] measurements. We note that Zimanyi *et al.*[15] have proposed a slightly higher completion coverage of 0.293 atom/Å^2.

TABLE IV. Energy/particle versus coverage at 400 mK with positions of both second- and third-layer atoms sampled. Calculations used the 5×3 simulation cell. The number in parentheses gives the error in the last two digits.

N	σ (Å^{-2})	E/N (K)
19	0.2075	−30.687(19)
20	0.2117	−30.111(13)
21	0.2159	−29.257(39)
24	0.2286	−27.391(20)
26	0.2371	−26.354(12)
27	0.2413	−25.937(12)
28	0.2456	−25.516(13)
31	0.2583	−24.462(21)
32	0.2625	−24.188(15)
33	0.2667	−23.910(13)
34	0.2710	−23.603(15)
35	0.2752	−23.314(13)
36	0.2794	−23.001(14)
37	0.2837	−22.699(12)
38	0.2879	−22.417(19)
40	0.2964	−21.816(13)

The layer promotion illustrated above is accompanied by a discontinuity in the chemical potential. We can obtain this quantity by differencing our calculated total energy values given in Table IV and plot the results in Fig. 14. Included in this figure are the results obtained for the second layer from a previous calculation.[4] As can be seen, there is a distinctive

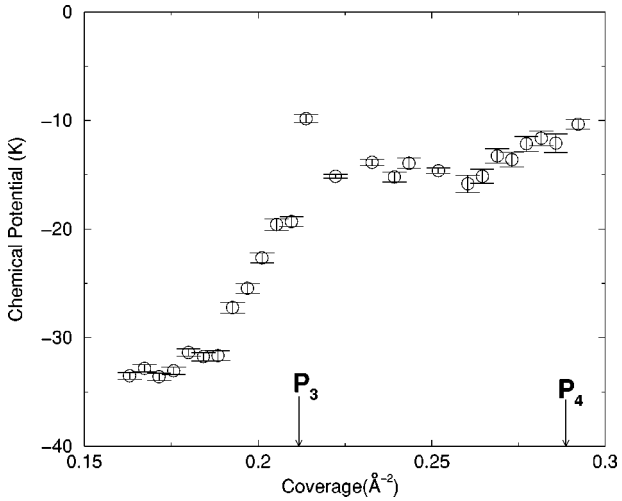

FIG. 14. Chemical potential for the second and third layers. The third layer and fourth-layer-promotion densities are indicated by the arrows.

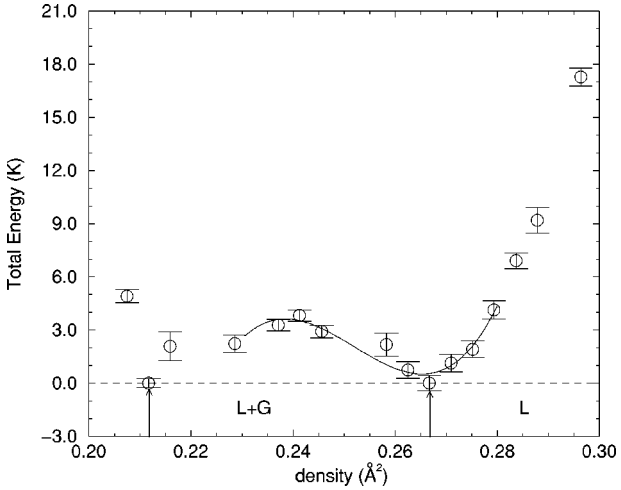

FIG. 15. Total energy at 400 mK for the three-layer system when the second-layer atoms are included in the sampling. The dashed line is the gas-liquid-coexistence line for the third layer. The arrows indicate the beginning of promotion to the third layer and the equilibrium third liquid coverage. Coverage ranges for the gas-liquid $(G+L)$ and uniform liquid (L) phase in the third layer are shown. The solid line is the fit to Eq. (2).

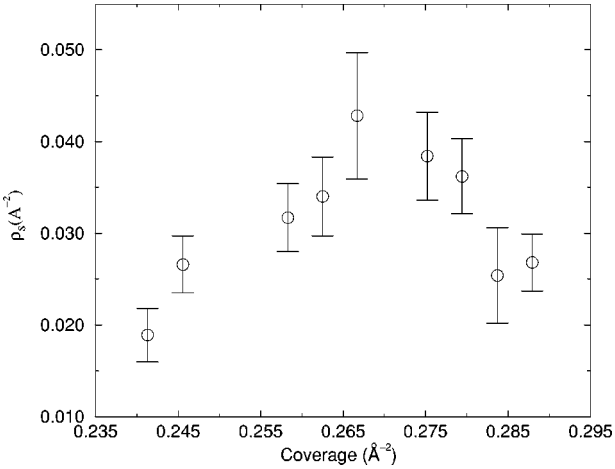

FIG. 16. Superfluid coverage for the third layer at 400 mK with both the second and third layer atoms sampled.

change in the density dependence of the chemical potential μ around the promotion density. Below the promotion density, the energy changes very rapidly with increasing coverage. Near promotion, an added atom has the choice of going to the unoccupied third layer or the dense second layer and will choose the layer that is energetically favorable. When the promotion coverage is reached, the chemical potential for adding the atom to the second layer exceeds that for adding it to the third layer and so the atom is added to the unoccupied layer. It can be seen from the figure that the change in μ associated with the promotion is quite large. In this case, the second layer is solid and relatively dense, so we expect an energy gap to be associated with promotion. As can be seen in the density profiles (see Fig. 13) for this layer, there is a range of heights above the second layer that is forbidden for the third-layer atom. This is in contrast to what happens in the case of fourth-layer promotion (see Fig. 2) in which there is significantly more overlap between the third and fourth layers. Each additional atom added to the system will also go the outer layer but the rate of the energy change will decrease since these atoms are attracted to each other and form a droplet. Thus we see that the chemical potential just after layer promotion decreases.

2. Layer phases

We can determine phase boundaries for the third layer by again using the Maxwell construction. Figure 15 gives the total-energy values for the three-layer system with both second and third layers active. The energy values per particle are given in Table IV. As before, a coexistence line can be drawn between the beginning of the third layer, 0.2117 atom/Å^2, and the equilibrium liquid coverage. The upper endpoint of the coexistence region is 0.2667 atom/Å^2. This is the equilibrium coverage for the third-layer liquid. The intermediate energy values are in gas-liquid coexistence. Following our usual procedure, we have subtracted out the gas-liquid coexistence line from all the energy values using the values -30.111 ± 0.019 K and -23.910 ± 0.013 K for the beginning (0.2117 atom/Å^2, 20 atoms) and end (0.2667 atom/Å^2, 33 atoms) of the coexistence region.

As with the results found using the frozen second layer, we can fit the energy values to a polynomial in the form of Eq. (2). This is the solid curve in Fig. 15. Energy values for the very low and high coverages of the layer were not included in the fit. The equilibrium coverage determined is 0.2653 ± 0.0005 atom/Å^2 and the spinodal point is found to be near the third layer coverage of 0.040 atom/Å^2.

At the temperature of our simulation, superfluidity can be observed in the third and fourth layers. Superfluid density values ranging from intermediate third layer to low fourth layer coverages are shown in Fig. 16. The values shown are the ratios of the superfluid density to the third layer coverage. Suppression of superfluidity before promotion to the fourth layer is found in our calculations. Figure 16 shows the superfluid coverage (instead of the superfluid fraction) versus the coverage for the third layer. In Ref. 4 we have reviewed how the superfluid density for such superfluid films is calculated using our PIMC method. Suppression of superfluidity has been observed at similar temperatures and coverage values in both the torsional oscillator measurements of Crowell and Reppy[1,2] and a simulation of helium on hydrogen.[26] Suppression just after fourth-layer promotion is a consequence of gas-liquid coexistence. In the low-coverage region, the fourth layer consists of droplets that lack the connectivity to exhibit superfluidity until they have percolated across the surface.[14,19] In addition, suppression of superfluidity before promotion to the fourth layer can be observed.

For superfluid films adsorbed on heterogeneous surfaces (such as Vycor), the superfluid coverage increases continuously with increasing coverage.[33] This does not occur in the atomically thin fluid layer we are simulating. Superfluidity instead increases with increasing coverage until the equilibrium density is reached after which there is a plateau and

then a drop. The drop in ρ_s is seen experimentally as well for coverages greater than 0.280.

The reason for the suppression of superfluid density before layer promotion is not clear but three related factors can contribute. First, increasing the density in the liquid layer produces excitations that should disrupt the superfluid state. This energy increase can be seen in Figs. 9 and 15. Second, increased correlation between the atoms will suppress the permutations required for superfluidity. We observe this increase in the radial distribution function, Fig. 6, and in the probability contours. The calculated probability distributions also suggest the third mechanism, namely, the layer is partially solidifying before layer promotion. As discussed above, we have not found clear evidence that this occurs.

IV. SUMMARY

This paper has presented path-integral Monte Carlo calculations for the third and fourth layers of helium on graphite using two different treatments of the underlying solid layers. In the first approach, we treated the first and second layers as inert. The second-layer solid was initially equilibrated and then atoms were frozen in some particular configuration. This simplification neglects the response of the second layer to the growth of the third layer as well as effects such as particle demotion but allows us to simulate larger systems. Using this approach, we have produced as many as three additional layers on top of the solid first and second layers. The third and fourth layers are found to possess self-bound liquid phases with layer densities of 0.0528 and 0.0508 atoms/Å^2, respectively. These densities are in agreement with the values that may be inferred from heat capacity and torsional-oscillator measurements. In the third layer, below the equilibrium density, we determine the spinodal point to be 0.0386 atoms/Å^2. This coverage separates the unstable region in which droplets form on the surface from the metastable ''stretched'' phase just before equilibrium. Static-structure calculations confirm that droplets occur at low densities. The chemical potential was also calculated and third-layer promotion was found to coincide with a discontinuity in the density dependence of this quantity. The superfluid density has been calculated for coverages from the third layer equilibrium to low fourth layer coverages. Promotion to the fourth layer is observed at the (total) coverage 0.2837 atoms/Å^2. The continued growth of the third layer is also observed after fourth-layer promotion. The question of partial solidification in this layer remains open for further investigation. In particular, it is possible that particle promotion preempts the formation of a third layer solid but particle demotions at higher coverages may increase the density of this layer to the point of solidification. Experimentally, there are some suggestive evidences for the third-layer solidification through compression by higher layers. We find that the heat capacity feature that emerges above 0.3100 atom/Å^2 (Ref. 8) might be related to the melting of this solid. Solidification also provides a natural explanation for the plateaus seen in torsional-oscillator measurements of the superfluid density of the higher layers.

The effects of including the second-layer atoms in the Monte Carlo updating procedure have also been examined. These calculations incorporate the effects of zero-point motion in the second-layer solid and allow this layer to respond to the third and higher layers. We observe particle demotion from the third to the second layer near equilibrium and again near the fourth-layer-promotion density. The overall coverage at which the third-layer liquid phase forms increases slightly from 0.2645 to 0.2653 atoms/Å^2 when the second layer is active. The completion density is also slightly higher, occurring at 0.2879 atoms/Å^2. A very notable effect produced by the active second layer was the reduction in the third-layer superfluid density at high coverages. This effect has also been seen experimentally.

ACKNOWLEDGMENTS

This work was supported by National Aeronautics and Space Administration (NASA) under Grant No. NAG3-1841. We wish to thank K. Nho for producing the data presented in Fig. 8.

[1] P. A. Crowell and J. D. Reppy, Phys. Rev. Lett. **70**, 3291 (1993).
[2] P. A. Crowell and J. D. Reppy, Phys. Rev. B **53**, 2701 (1996).
[3] M. Pierce and E. Manousakis, Phys. Rev. Lett. **81**, 156 (1998).
[4] M. Pierce and E. Manousakis, Phys. Rev. B **59**, 3802 (1999).
[5] R. E. Ecke, Q.-S. Shu, T. S. Sullivan, and O. E. Vilches, Phys. Rev. B **31**, 448 (1985).
[6] M. Pierce and E. Manousakis, Phys. Rev. Lett. **83**, 5314 (1999).
[7] M. Pierce and E. Manousakis, Phys. Rev. B **62**, 5228 (2000).
[8] D. S. Greywall, Phys. Rev. B **47**, 309 (1993).
[9] J. M. Gottlieb and L. W. Bruch, Phys. Rev. B **48**, 3943 (1993).
[10] L. W. Bruch, M. W. Cole, and E. Zaremba, *Physical Adsorption: Forces and Phenomena* (Oxford, New York, 1997).
[11] D. S. Greywall and P. A. Busch, Phys. Rev. Lett. **67**, 3535 (1991).
[12] J. Nyéki, R. Ray, B. Cowan, and J. Saunders, Phys. Rev. Lett. **81**, 152 (1998).
[13] G. Zimmerli, G. Mistura, and M. H. W. Chan, Phys. Rev. Lett. **68**, 60 (1992).
[14] J. G. Dash, Phys. Rev. Lett. **41**, 1178 (1978).
[15] G. T. Zimanyi, P. A. Crowell, R. T. Scalettar, and G. G. Batrouni, Phys. Rev. B **50**, 6515 (1994).
[16] B. E. Clements, E. Krotcheck, and H. J. Lauter, Phys. Rev. Lett. **70**, 1287 (1993).
[17] B. E. Clements, J. L. Epstein, E. Krotcheck, and M. Saarela, Phys. Rev. B **48**, 7450 (1993).
[18] W. M. Saslow, G. Agnolet, C. E. Campbell, B. E. Clements, and K. Krotcheck, Phys. Rev. B **54**, 6532 (1996).
[19] C. E. Campbell, B. E. Clements, E. Krotscheck, and M. Saarela, Phys. Rev. B **55**, 3769 (1997).
[20] N. Pavloff and J. Treiner, J. Low Temp. Phys. **83**, 331 (1991).
[21] E. Cheng, M. W. Cole, W. F. Saam, and J. Treiner, Phys. Rev. B **46**, 13 967 (1992).

[22] E. Cheng, M. W. Cole, J. Dupont-Roc, W. F. Saam, and J. Treiner, Rev. Mod. Phys. **65**, 557 (1993).
[23] F. F. Abraham and J. Q. Broughton, Phys. Rev. Lett. **59**, 64 (1987).
[24] F. F. Abraham, J. Q. Broughton, P. W. Leung, and V. Elser, Europhys. Lett. **12**, 107 (1990).
[25] M. Wagner and D. M. Ceperley, J. Low Temp. Phys. **94**, 171 (1994).
[26] M. Wagner and D. M. Ceperley, J. Low Temp. Phys. **94**, 185 (1994).
[27] D. M. Ceperley, Rev. Mod. Phys. **67**, 279 (1995).
[28] K. Carneiro, L. Passell, W. Thomlinson, and H. Taub, Phys. Rev. B **24**, 1170 (1981).
[29] J. G. Dash, *Films on Solid Surfaces* (Academic, New York, 1975).
[30] P. A. Whitlock, G. V. Chester, and M. H. Kalos, Phys. Rev. B **38**, 2418 (1988).
[31] H. J. Lauter, H. Godfrin, V. L. P. Frank, and P. Leiderer, in *Phase Transitions in Surface Films 2*, edited by H. Taub, G. Torzo, H. J. Lauter, and S. C. Fain (Plenum, New York, 1991).
[32] S. E. Polanco and M. Bretz, Phys. Rev. B **17**, 151 (1978).
[33] J. D. Reppy, in *Phase Transitions in Surface Films*, edited by J. G. Dash and J. Ruvalds (Plenum, New York, 1980).